ENHANCEMENT OF Li–ION BATTERY CAPACITY USING NICKEL DOPED $LiFePO_4$ AS CATHODE MATERIAL

La Thi Hang[1, 2, 3, *], Le My Loan Phung[4], Nguyen Thi My Anh[5], Hoang Xuan Tung[5], Doan Phuc Luan[5], Nguyen Nhi Tru[5]

[1]Vinh Long University of Technology Education (VLUTE)
73 Nguyen Hue Street, Vinh Long City, Vinh Long Province, Vietnam
[2] Institute of Applied Materials Science – VAST
1 Mac Dinh Chi Street, Ben Nghe Ward,, District 1, Ho Chi Minh City, Vietnam
[3] Graduate University of Science & Technology – VAST
18 Hoang Quoc Viet Street, Nghia Do Ward, Cau Giay District, Hanoi, Vietnam
[4]Applied Physical Chemistry Lab, University of Science – VNU HCM
227 Nguyen Van Cu Street, Ward 4, District 5, Ho Chi Minh City, Vietnam
[5] Faculty of Materials Technology, University of Technology – VNU HCM
268 Ly Thuong Kiet Street, Ward 14, District 10, Ho Chi Minh City, Vietnam

[*]Email: *hanglt@vlute.edu.vn*

Received: 30 December 2016; Accepted for Publication: …

ABSTRACT

Selective supervalent cations (M = Ni, Mn, La etc.) doped $LiFePO_4$ (LFP) is an effective route to enhance its electrical conductivity, thereby improving electrochemical performances of lithium–ion batteries. For this purpose, nickel doped $LiFePO_4$ based cathode material was investigated at different substitution amounts (x_{Ni} = 0.05, 0.10). $LiFe_{1-x}Ni_xPO_4$ (LFNP) was synthesized from $Ni(NO_3)_2.6H_2O$, $LiOH.H_2O$, $FeSO_4.7H_2O$, H_3PO_4, and ascorbic acid precursors via solvothermal technique, followed by calcination in nitrogen atmosphere at 550 °C for 5 h. The structure and morphology of synthesized materials were examined by X–ray diffraction, Scanning electronic microscopy and Raman vibrational micro–spectroscopy. The electrochemical performances of doped materials were studied in Swagelok–type cell using $LiPF_6$/EC–DMC (1:1) as electrolyte. $LiFe_{1-x}Ni_xPO_4$ was shown to exhibit homogenous particles size of 50 ÷ 150 nm. The doped materials were titrated to quantify iron and nickel contents in samples. As anticipated, the electrochemical performances of $LiFe_{1-x}Ni_xPO_4$were significantly enhanced compared to those of undoped $LiFePO_4$.

Keywords: $LiFe_{1-x}Ni_xPO_4$ (LFNP), solvothermal, lithium–ion, conductivity, capacity.

1. INTRODUCTION

$LiFePO_4$(LFP) is a promising cathode material for manufacturing lithium–ion batteries with prolonged life time, good cycle stability, environmental friendliness, and relatively low cost.

However, due to its rigid orthorhombic olivine structure, the intrinsic electronic conductivity of LFP and Li^+ diffusion rate is considerably low to reach full theoretical capacity during battery operation [1–3]. Different technical approaches have been used to overcome these drawbacks, such as: doping LFP with supervalent cations [3–5], reduction of particle size to nanoscale [3, 6] and/or particle coating with carbon based materials [7, 8].

By doping way, the enhancement of LFP electrochemical capacity has been reported with promising results. By titanium doping, Wu L. et al. [1] observed LFP capacity increase from125 to 150 Ah/kg at 0.1C discharge rate. Göktepe H. et al. [8] reported the electronic conductivity of 1.9×10^{-3} S/cm and capacity of 146 Ah/kg obtained by combining Yb^{3+} doped and carbon coated LFP to form $LiYb_{0.02}Fe_{0.98}PO_4/C$ composite. Similarly, through the variation of lanthanum amounts doped in LFP, Cho et al. [9] found out that with 1% lanthanum content ($LiFe_{0.99}La_{0.01}PO_4/C$), the LFP structure remained unchanged, meanwhile, its capacity increased from 104 to 156 Ah/kg at 0.2C discharge rate and exhibited good cycling stability. Furthermore, Li et al. [10] examined manganese doped $LiMn_xFe_{1-x}PO_4$ with $0.1 \leq x \leq 0.9$, the highest energy density of 595 Wh/kg was obtained at x = 0.75. Finally, LFP doping with supervalent cations can be conducted via solvothermal method to form relatively pure product with controllable particle sizes [6].

Selection of non–toxic, inexpensive, and naturally affordable (abundant) doping metals is a common strategy to enhance performance of cathode materials. Currently, nickel has been usually applied based on these requirements, comparing to widely used cobalt in lithium ion battery [4, 5, 7, 8]. Furthermore, in LFP structure, P–O bond is flexible compared to the Fe–O bonding. Replacement of iron (r_{Fe} = 140 nm) by nickel with relatively smaller atomic radius (r_{Ni} = 135 nm) in the crystalline network, can narrow the band gap and depress the rigidity structure to favor the lithium ion diffusion pathway [4]. Besides, nickel (Z = 28: $3d^84s^2$) as d sub–orbital element with a number of unpaired electrons can easily participate in chemical bonding. Finally, the redox potentials shifting to the higher value is also revealed after doping, which can be explained by changes in the Me–O covalent bonding such as: change in electronegativity of Me ion, Me–O bond length, by the influence of the Me–O–Me interactions in the solid composition [4, 11].

Nickel doping at 1–10% range was mentioned in various research works [10, 12]. According to [10], with > 10% doping, the iron replaced olivine structure tends to form defects; meanwhile, with < 5% doping, the XRD analysis could appear in a low detectable range, hinder the following structure interpretation. Thereby, a range of 5–10% nickel doping could be considered acceptable to examine the possibility of LFNP solvothermal synthesis and enhancement of lithium–ion battery performance.

In this paper, the nickel doped LFP is prepared via solvothermal reaction with different nickel amounts; the effect of nickel doping on LFP structure and electrochemical properties are reported and discussed.

2. MATERIALS AND METHODS

2.1. Synthesis of $LiFe_{1-x}Ni_xPO_4$

The starting reagents as $Ni(NO_3)_2.6H_2O$ (Merck, Germany), $LiOH.H_2O$ (Fisher, Belgium), $FeSO_4.7H_2O$ (Merck, Germany), H_3PO_4 (Merck, Germany), $C_6H_8O_6$ (Fisher, Belgium), ethylene glycol (Merck, Germany) of analytical grade were used for synthesis. The Li:Fe:Ni:P mass ratios were calculated, respectively: 3:0.9:0.1:1 and 3:0.95:0.05:1 for $LiFe_{0.95}Ni_{0.05}PO_4$ and

$LiFe_{0.9}Ni_{0.1}PO_4$. Firstly, $LiOH.H_2O$ was dissolved in 40 mL ethylene glycol under ultra–sonication until clear solution was obtained. The $FeSO_4.7H_2O$ and $Ni(NO_3)_2.6H_2O$ mixture was then separately dissolved in 60 mL ethylene glycol under nitrogen atmosphere for 15 min. Then, the ascorbic acid was slowly added to totally reduce Fe^{3+} into Fe^{2+} to form a homogenous light green solution. The H_3PO_4 solution (85 wt%) was continuously dropped into light green solution and kept stirring in 30 min. The solution was finally transferred into autoclave under the argon atmosphere to perform the solvothermal reaction in 180 °C for 5 h. After reaction, the greyish precipitate was centrifuged, rinsed repeatedly with ethanol and dried in vacuum at 70 °C for 7–9 h. The sample was finally calcined at 550–600 °C in nitrogen atmosphere for 5 h to remove impurities.

2.2. Material analysis and characterization

Iron contents in LFP and nickel doped LFP were analyzed by volumetric titration method using $KMnO_4$ in concentrated H_2SO_4 medium to fully oxidize Fe^{2+} into Fe^{3+}. The LFP and LFNP samples were stirred with 50 mL H_2SO_4 until formation of clear green solution. The solution was then titrated with 0.0125N $KMnO_4$.

Raman measurements were performed using Horiba Jobin Yvon LabRAM HR300 system (at Institute of Nanotechnology – VNUHCM) with 514.5 nm laser radiation. With 1 μm penetration, the vibration of LFNP bonds was determined and its structure was identified.

The LFNP crystalline structure, phase purity and the particles size were characterized using a Rigaku/max 2500Pc and D8 Brucker X–ray diffractometer (XRD) with Cu–Kα radiation (λ=1.5418 Å, 2θ: 10° to 170° at a scan rate 0.25°/s – 1.00°/s). Analysis was performed at Center for Molecular and Nanoarchitecture, Ho Chi Minh city. Scanning electron microscopy (SEM) with Hitachi SEM S4800–NHE equipment was used to characterize the composite morphology. The measurements were conducted in the National Institute of Hygiene and Epidemiology.

The LFNP powder was mixed with acetylene black and copolymer binder (PVdF–HFP) (weight ratio 80:10:10) in N–methyl pyrrolidone (NMP). The ink solution was pasted on the aluminum foil with 0.1 mm thickness and dried in vacuum for 24 h. A charge/discharge cycling test for Swagelok–type battery was carried out in liquid electrolyte $LiPF_6$/EC–DMC (1:1) at room temperature. Cells were assembled in a glove box under argon atmosphere with < 2 ppm H_2O. Electrochemical studies were carried out using a MPG2 Galvano/Potentiostat (Bio–Logic, France; Applied Physical Chemistry Laboratory, Univesity of Science, VNUHCM) in the potential window of 3.0 – 4.2 V versus Li/Li^+ in the galvanostatic mode at the C/10 regime.

3. RESULTS AND DISCUSSION

3.1. Determination of iron content in LFP and LFNP samples

The volumetric titration results of Fe^{2+} content in the LFP and LFNP shows in equation (1). The iron content (in gram) was calculated using equation (2).

$$5Fe^{2+} + MnO_4^- + 8H^+ \rightarrow 5Fe^{3+} + Mn^{2+} + 4H_2O \quad (1)$$

$$\boldsymbol{m_{Fe} = 5 \times C_{KMnO4} \times V_{KMnO4} \times 56 \times 10^{-3}} \quad (2)$$

Suppose that all iron content is converted equivalently to Fe^{2+}, theoretically, with LFP sample, an initial stoichiometry of Li: Fe: P = 3:1:1, the percentage of Fe content (%) in LFP samples can be calculated by following equation (3):

$$\%\boldsymbol{Fe(LFP)} = \frac{\boldsymbol{56X}}{\boldsymbol{7x3X+56X+95X}} \times \mathbf{100} = \mathbf{32.56\%}\ \ (\boldsymbol{with\ X: mol}) \quad (3)$$

Similarly, iron contents were calculated for $LiFe_{0.9}Ni_{0.1}PO_4$ and $LiFe_{0.95}Ni_{0.05}PO_4$ as 29.30% and 30.28% respectively (Table 1).

In Table 1, the correlation between the calculated and experimentally analyzed results is clearly observed for LFP and LFNP with acceptable deviation. The iron amount in $LiFePO_4$ is higher than in $LiFe_{0.9}Ni_{0.1}PO_4$ and $LiFe_{0.95}Ni_{0.05}PO_4$ samples due to its 7÷10 wt% replaced by nickel doped in the structure.

Table 1. Iron content in LFP and LFNP determined by volumetric titration.

Sample	$KMnO_4/H_2SO_4$ titrated volume (mL)	Iron content in the sample (g)	Iron content in the samples (%)		
			Analyzed	Calculated	Deviation
$LiFePO_4$	23.0	0.0805	30.53	32.56	6.2
$LiFe_{0.95}Ni_{0.05}PO_4$	19.0	0.0665	**25.21**	**29.30**	14.0
$LiFe_{0.9}Ni_{0.1}PO_4$	18.5	0.0648	**24.55**	**30.28**	19.0

3.2. Structural characterization

The XRD patterns of LFP and LFNP solvothermally synthesized with 5 and 10% nickel contents presented in Figure 1 are similar. The XRD patterns indicate an orthorhombic structure with space group Pnma (JCPDS 96–101–1112). Thereby, the nickel insertion did not influence on LFP olivine structure. However, the red shift of XRD patterns for doped samples indicates the contraction of lattice parameters.

A considerable shift of XRD peaks after nickel doping can be explained as follow: As a multivalent element, iron is easily oxidized during solvothermal synthesis, result a LFP product with low crystalline peaks [6]. Nickel replacement can eliminate iron oxidation, favoring the product formation with peaks of higher intensity, compared to undoped LFP.

Furthermore, the particle sizes were estimated as 20÷60 nm using the Scherrer formula with $\beta\cos\theta = k\lambda/D$, where β is the full–width–at–half–maximum length of the diffraction peak on a 2θ scale and k is a close to unit constant.

The lattice parameters can be estimated using XRD patterns data and the cell volume can also be deduced from orthorhombic (olivine) structure (Eq. 4). Within orthorhombic or cubic lattice, the α, β, γ values are assigned to 90^o.

$$\boldsymbol{V = abc\sqrt{1 + 2\cos(\alpha)\cos(\beta)\cos(\gamma) - \cos(\alpha^2) - \cos(\beta^2) - \cos(\gamma^2)}} \quad (4)$$

It is clearly from Table 2, the lattice parameters (values of a, b, c) of undoped LFP is slightly decreased by nickel doping. The decrease of cell parameters is explained by replacement of iron Fe^{2+} (r_{Fe}^{2+} = 125 Å) by smaller Ni^{2+} ion (r_{Ni}^{2+} = 121 Å). It proves that nickel has been successfully doped into structure and partly replaced in the M_1 sites (Li) or M_2 sites (Fe) without impact on the olivine structure.

Furthermore, the electronic conductivity of the materials could indirectly be determined from equations Q = I.t and L= 1/R (with Q: capacity, I: current; t: time (h), L: conductivity (S/cm), R: impedance (Ohm) [4] and experimental derived from electrochemical measurement data and calculated results in Table 2 show significant increase of conductivity for synthesized LFNP comparing to LFP (approx. 2 times).

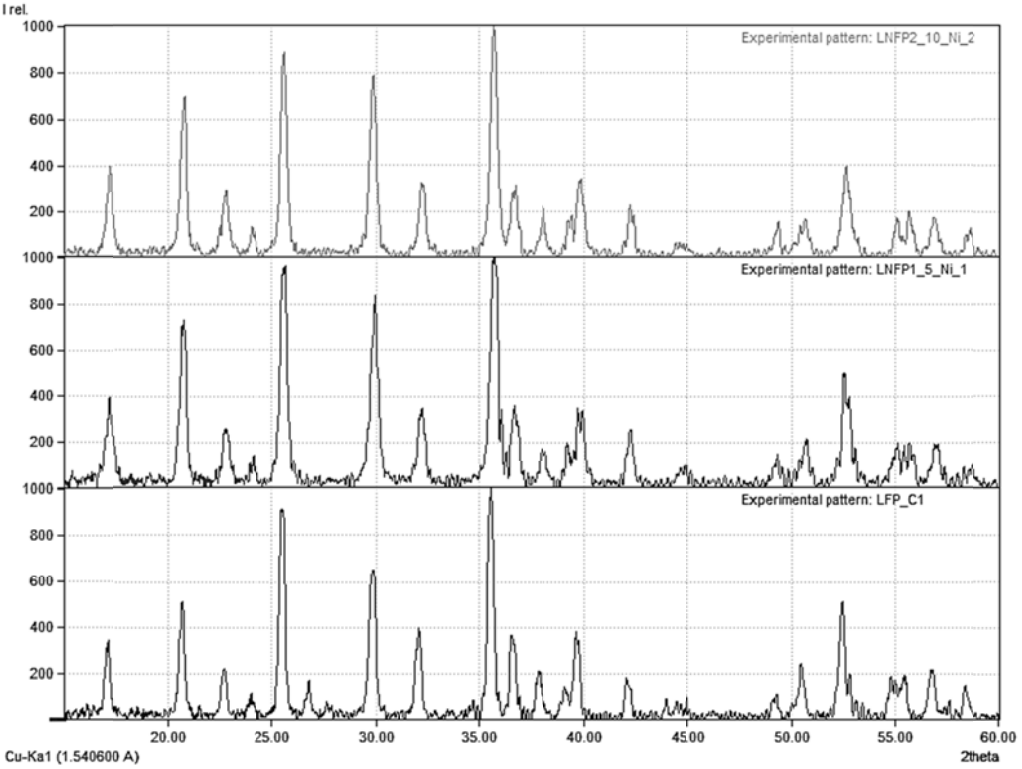

Figure 1. Comparative XRD patterns of undoped and nickel doped (5 and 10%) LFP samples.

Table 2. Data of lattice parameters and conductivity calculated for LFP and LFNP samples.

Samples	Lattice parameters (Å)			Volume (Å^3)	Conductivity (S/cm)
	a	*b*	*c*		
LFP (synthesized)	10.335	6.004	4.698	291.5	1.0×10^{-3}
$LiFe_{0.95}Ni_{0.05}PO_4$	10.087	5.885	4.682	277.9	2.3×10^{-3}
$LiFe_{0.9}Ni_{0.1}PO_4$	10.080	5.875	4.678	277.0	2.5×10^{-3}

The vibration features of olivine–type compound (space group D_{2h} ^{16}Pnma) were documented in the literature [11]. Those vibrations are classified into internal and external modes. The internal modes (ν1, ν2, ν3, ν4) refer to vibrations occurring in the PO_4^{3-} tetrahedral and the external ones are pseudo–rotations and translations of the units. Among these, the internal vibrations in terms of symmetry species are A1(ν1) symmetric P–O stretching, E(ν2) symmetric O–P–O bond bending, F2(ν3) antisymmetric P–O stretching, and F2(ν4) antisymmetric O–P–O bond bending. The translations include motions of the center of mass PO_4^{3-} and M^{2+}. It should be mentioned that this separation is a guide to discussion only, because the vibrations may be coupled. In Figure 2, Raman spectroscopy showed typically LFP vibrational bands, respectively 150–300 cm^{-1} (translation modes, T); 570–650 cm^{-1} (ν4 modes), 900–1200 cm^{-1} (ν3 modes). Nickel doped LFP suppressed the translation modes at 150–300 cm^{-1} as well as internal mode (ν4). The separation of ν4 modes at 995 cm^{-1} and 1067 cm^{-1} was observed in the doped sample. In addition, the appearance of new vibration bands at 1340–1610 cm^{-1} is assigned to the D, G bands of graphite coating in case of nickel doped LFP.

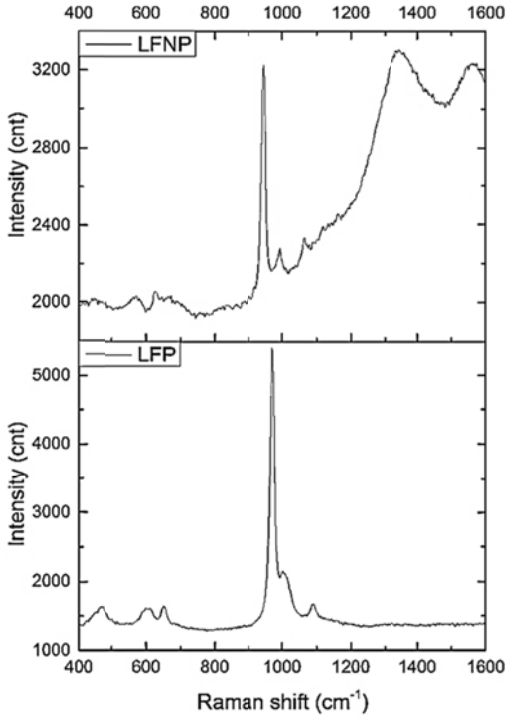

Figure 2. Comparison of Raman spectra between LFNP and LFP (after calcination at 550 °C).

3.3. Particle sizes and morphology characterization

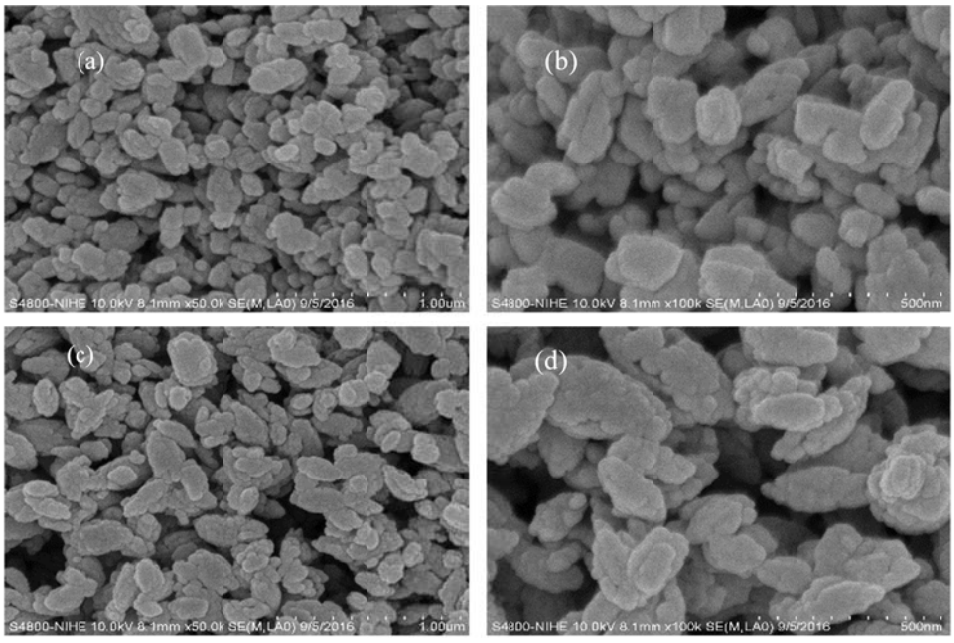

Figure 3. SEM images of LFNP with 10% of Ni (a; b) and 5% of Ni (c; d) samples synthesized via solvothermal technique.

The morphology and particles sizes were determined by SEM images. Figure 3 shows relatively homogenous particle shapes and size distribution of LFNP particles ranging from 50 to 150 nm; The increase of nickel doping amount suppressed partly the agglomeration of particles.

3.4 Characterization of electrochemical performances

Figure 4 compares the initial charge – discharge voltage profile of LFP and LFNP electrodes (x_{Ni} = 0.05; 0.10) at scan rate of C/10. All the samples have similar charge – discharge curve with flat plateaus corresponding to the lithium intercalation/de–intercalation in/out the olivine structure. The nickel doped LFP enhanced the charge – discharge voltage, typically 3.6 V towards 3.5 V for pure LFP in charge, and 3.4 V towards 3.5 V in discharge. Additionally, the significant increase of specific capacity was observed for LFNP samples. Thus, the doped nickel could enhance electronic conductivity and lithium diffusion rate which improve the capacity and cycle life of batteries.

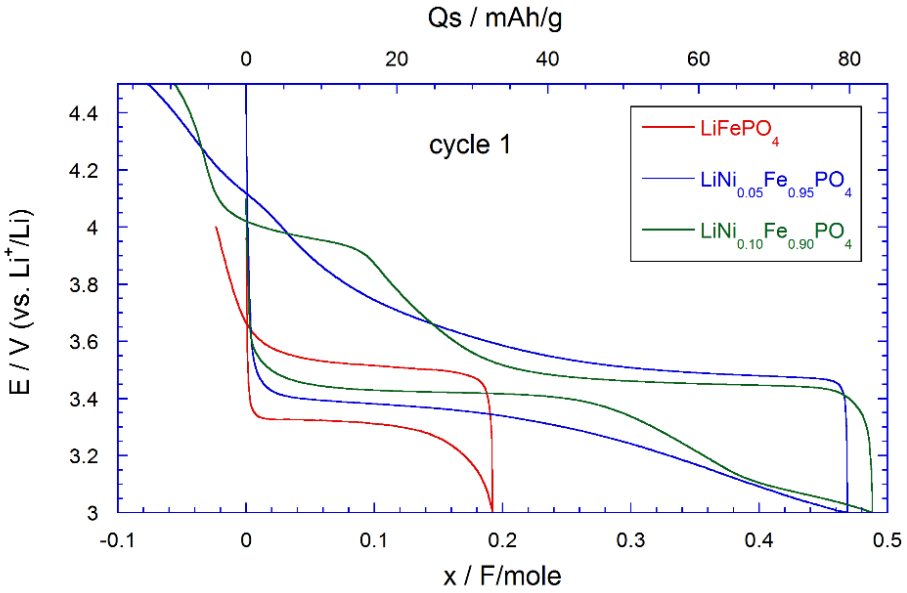

Figure 4. Initial charge – discharge curve at C/10 of LFP and LFNP samples.

4. CONCLUSIONS

$LiFePO_4$ and nickel doped samples were successfully synthesized using solvothermal technique. The nickel impact on LFP structure clearly exhibited by the decrease of volume and lattice cell parameter as well as suppression of some vibration bands (translation and internal modes). The capacity and voltage of doped samples enhanced significantly due to increase of electric conductivity and lithium diffusion rate. The results would be further on the aspect of structure evolution during charge – discharge to understand the diffusion pathway.

Acknowledgements. This work was financially supported by Ho Chi Minh City University of Technology & Vietnam National University of Ho Chi Minh City through the Science and Technology Funds granted for C2015–20–25 Project.

REFERENCES

1. Wu L., Wang Z. X., Li X. H., Li L. J., Guo H. J., Zheng J. C., Wang X. J. – Electrochemical performance of Ti^{4+}–doped $LiFePO_4$ synthesized by co–precipitation and post–sintering method, Transactions of Nonferrous Metals Society of China **20** (2010) 814–818.
2. Long Y., Shu Y., Ma X. H., Ye M. X. – *In–situ* synthesizing superior high–rate $LiFePO_4$/C nanorods embedded in graphene matrix, Electrochimica Acta **117** (2014) 105–112.
3. Hu J. Z., Xie J., Zhao X. B., Yu H. M., Zhou X., Cao G. S., Tu J. P. – Doping effects on electronic conductivity and electrochemical performance of $LiFePO_4$, Journal of Materials Science & Technology **25** (3) (2009) 405–409.
4. Dahlin G. R., E. Strom K. E. – Lithium batteries, Research and Applications, Publishers: Nova Science. Inc. New York, 2016, pp. 226.
5. Ziółkowska D., Korona K. P., Kamińska M., Grzanka E., Andrzejczuk M., Wu S. H., Chen M. – Raman spectroscopy of $LiFePO_4$ and $Li_3V_2(PO_4)_3$ prepared as cathode materials, Acta Physica Polonica **120** (5) (2011) 973–975.
6. La T. H., Nguyen N. T., Nguyen T. M. A., Le M. L. P., Doan L. V., Doan P. L. – Microwave–assisted solvothermal synthesis of $LiFePO_4$/C nanostructure for lithium ion batteries, Proceedings of the 5th Asian Materials Data Symposium, Hanoi – Vietnam (2016) 343–352.
7. Satyavani T. V. S. L., Srinivas Kumar A. S., Subba Rao P. S. V. – Methods of synthesis and performance improvement of lithium iron phosphate for high rate Li–ion batteries: A review, Engineering Science and Technology, an International Journal **19** (2016) 178–188.
8. Göktepe H. – Electrochemical performance of Yb–doped Li– $LiFePO_4$/C composites as cathode materials for lithium–ion batteries, Research on Chemical Intermediates **39** (3) (2013) 2979–2987.
9. Cho Y. D., Fey G. T. –K., Kao H. M. – Physical and electrochemical properties of La–doped $LiFePO_4$/C composites as cathode materials for lithium–ion batteries, Journal of Solid State Electrochemistry **12** (2008) 815–823.
10. Li G., Azuma H., Tohda M. – Optimized $LiMn_yFe_{1-y}PO_4$ as the cathode for lithium batteries, Journal of the Electrochemical Society **149 (**2002) A743–A747.
11. Baddour–Hadjean R., Pereira–Ramos J. P. – Raman microspectrometry applied to the study of electrode materials for lithium batteries, Chemical Reviews **110** (2010) 1278–1319.
12. Ge Y. C., Yan X. D., Liu J., Zhang X. F., Wang J. W., He X. G., Wang R. S., Xie H. M. – An optimized Ni doped $LiFePO_4$/C nanocomposite with excellent rate performance, Electrochimica Acta **55** (2010) 5886–5890.